THE PENNSYLVANIA STATE UNIVERSITY

PROGRESS REPORT NO. 11

HIGH PRESSURE IGNITION

CONTRACT NO. Nobs 78674

June 28, 1962

COLLEGE OF ENGINEERING AND ARCHITECTURE

DEPARTMENT OF MECHANICAL ENGINEERING

(5) 690 300

Research was continued on a study of the physical processes which govern the ignition, by rapid compression, of hydraulic fluids.

PROGRESS REPORT NO. 11 (16-19) NA

TO: Chief, Bureau of Ships
Department of the Navy
Washington 25, D.C.

Attn: Code 634 A (20) U (21) NA

FROM: Department of Mechanical Engineering (7-8) NA
The Pennsylvania State University
University Park, Pennsylvania

SUBJECT: (Upper case) (6) Ignition of Hydraulic Fluids in High Pressure Pipe Systems. (15) Contract [redacted] NObs 78674

~~(This report covers the period 1 April to 31 May, 1962.~~

(9) Progress rept. no. 11, 1 Apr - 31 May 62,

I. Summary: (10) (11) 28 Jun 62, (13-14) NA

by G.M. Faeth.

1.) Maximum gas temperature calculations ~~have~~ were ~~been~~ completed for the 7/8 inch I.D. test section. The results of these calculations are shown in Fig. 1. (12) IV.

2.) Combustion tests were completed for Cetane and Mil 2190 TEP in the 7/8 inch I.D. test section. Two methods of fuel introduction were used, microfog and a wick saturated with the test fluid. The results of these tests are summarized in Figs. 2 and 3.

3.) By employing SIT data for Mil 2190 as given in Ref. 4 a combustion limit curve has been calculated for this fluid in the 7/8 inch I.D. test section. A comparison of the calculated curve with experimental results is shown in Fig. 4. The calculated curve is somewhat more conservative than the experimental results as would be expected.

4.) The combustion test modifications ~~have~~ were ~~been~~ completed for the 3/8 inch and 1 1/2 inch I.D. test sections.

~~5.)~~ An analysis for the case where the charging process is ~~has been~~ was made for the liquid charging case. Expressions for predicting the pressure vs. time curve and the maximum pressure rise rate were derived and show good agreement with test results. Also see AD 417599 to 417608 and AD 417610 to 417614.

II. Maximum Gas Temperature Calculations

For the maximum gas temperature calculations the analysis given in Ref. 1 was employed. The convection correlation used in the analysis was that derived in Ref. 2 for combined free and forced convection. For these calculations the following supplementary assumptions were made:

1.) The effect of axial heat conduction is negligable.

2.) The maximum gas temperature is attained at the center of the fluid increment extending one foot upstream of the end plate prior to the compression process.

As pointed out previously (Refs. 1 and 2) both these assumptions are consistent with the experimental results obtained to date.

The calculations assume an initial gas and pipe wall temperature of 80°F with the initial pressure in the downstream pipe being 14.2 psia which corresponds to the average conditions in this laboratory.

The calculation procedure was as follows:

1.) A pressure rise rate was selected.

2.) The calculation proceeded step by step with the gas temperature at the center of the increment being recorded as a function of gas pressure.

3.) This procedure was continued until a point was reached where the gas temperature began to decrease as the pressure increased. The maximum temperature attained at any pressure higher than the pressure at which the gas temperature began to decline was taken as being the maximum temperature given by calculation.

By continuing this process for a variety of pressure rise rates eventually enough data were accumulated to allow a plot of constant temperature lines with respect to pressure rise and maximum pressure. The results are shown in Fig. 1 for the gas temperature range between 250 and 900°F, which is the most critical temperature region in regard to spontaneous ignition.

The interpolation for plotting constant lines was alone on semi-log paper in order to take into account the exponential change in temperature with a linear change in pressure.

II. Combustion Tests

2.1 Test Procedure

The 7/8 inch I.D. test section was employed for these tests, the test section being 5 feet lone and in a horizontal position.

The procedure for conducting the miscofog tests has already been outlined in Ref.3.

For the wick tests a small piece of fiberglass cloth was attached to a post along the centerline of the test section, extending from the end plate to 1/2 inch upstream. Prior to a test this wick was saturated with a measured quantity of the test fluid, applied with a hypodermic needle. Whether combustion occurred or not the wick was replaced after each test. Ignition was detected both by the photocell and by visual observation of the wick following a test. In all instances these two methods of ignition were in complete agreement.

For both forms of fluid introduction a test condition was only noted as a point of no ignition if ignition failed to occur for 4 tests.

2.2 Test Results

The results of the Cetane and Mil 2190 TEP tests are plotted in Figs. 2 and 3 respectively. For both of these figures microfog ignition is denoted by the symbol (●) and ignition with the wick by (▲), points of no ignition are indicated by the same symbols (○, △) not blacked in.

The line issuing from the origin of the coordinate system and slanting upward and to the right is the pressure rise rate limit line. The line denotes the maximum attainable pressure rise rate for a given final pressure with the present test configuration.

The microfog tests with Cetane were conducted with an overall air-fuel ratio of 59. Further tests were made using higher air-fuel ratios with no change in the results shown in Fig. 2 until the air fuel ratio reached 180 above which slightly higher final pressures and pressure rise rates were necessary for ignition. The microfog tests with Mil 2190 TEP were conducted with an overall air-fuel ratio of 113 which was the lowest that could be attained for this fluid with the present microfog unit. In this case detectable variations in the combustion limit curve were noted when the air fuel ratio reached 200.

2.3 Discussion

The fact that the mode of fluid introduction has a different effect on different pressure ranges points out the necessity of including both microfog and wick tests in order to find the most conservative results. Whether some other form of fluid introduction would give more conservative results remains an open question. The physical reason for such behavior is not yet apparent and it is hoped that the work to be undertaken in the next few months will help to clarify this picture somewhat.

Although the results of the present tests with Mil 2190 TEP and those completed by Electric Boat Division as replotted in Ref. 4 are not strictly comparable due to difference in pipe diameters and maximum pressure it is of interest to note that the minimum pressure rise rates for combustion are of about the same order of magnitude. The present results are not as conservative which would be expected due to the higher heat losses in the smaller pipe and the increase in combustion resistance at lower pressures as evidenced by the Self Ignition Temperature (S.I.T.) curve for Mil 2190 TEP.

Employing the data on the S.I.T. of Mil 2190 TEP at various pressures as given in Ref. 4, a theoretical combustion limit curve was determined for this fluid. For this determination the isotherms of Fig. 1 were employed, assuming that combustion would occur at a given pressure when the gas temperature reached the S.I.T. This result is shown in Fig. 4 where the experimentally determined combustion limit curve for the wick tests is also included for comparison.

As would be expected, the theoretical curve is somewhat more conservative than the experimental one. This is due to the fact that the ignition lag is entirely neglected in the analysis and also because the calculated temperature given by the analysis of Ref. 1 have always been above the measured temperature.

III. Liquid Changing Study

3.1 Analysis

An analysis has been developed and is presented in the Appendix, for the case where the charging process is governed only by entrance and throttling losses. Two cases were considered: (1) the air column is compressed isentropically (2) the air is compressed isothermally.

The assumptions made throughout the analysis are as follows:

(A) Air Column

(1) A linearized representation of the isentropic compression process is used.

(2) The ratio of specific heats, K, is assumed constant and equal to 1.40.

(B) Charging Liquid

(1) The density of the liquid remains constant.

(2) The pressure and velocity of the liquid are assumed uniform across any cross section except in the immediate vicinity of the orifice and the entrance to the upstream pipe.

(3) The effects of fluid acceleration are neglected.

(4) Friction forces exerted on the liquid by the pipe walls are neglected.

(5) The coefficient of discharge of the orifice is assumed equal to 1.0.

(6) Quasi-steady state conditions are assumed at the orifice.

(7) Changes in elevation are neglected.

(8) The valve opens instantaneously.

(C) Air in the Storage Tank

(1) The air is expanded isentropically.

(2) During the process the change in air volume in the tank is negligible.

The analysis provides a method for predicting the pressure vs. time curve and the maximum pressure rise rate.

The equations for predicting the pressure vs. time curve are: (in the notation given in the Appendix)

$$\frac{C_1\sqrt{C_2}}{C_4}\left[-\frac{\cos\theta}{\sin^2\theta}+\ln\left(\tan\frac{\theta}{2}\right)\right]+\sqrt{C_2}\left[\frac{C_3}{C_4}\sqrt{1-\frac{C_1}{C_3}}+\frac{C_1}{C_3}\ln\frac{\sqrt{\frac{C_1}{C_3}}}{1+\sqrt{1-\frac{C_1}{C_3}}}\right]=t^* \qquad (1)$$

$$\sin^2\theta = \frac{P_g}{P_0} \quad , \quad \sin^{-1}\sqrt{\frac{C_1}{C_3}} \leqq \theta \leqq \frac{\pi}{2} \tag{2}$$

where:

$$C_1 = \frac{P_{g_0}}{P_{D_0}} \quad , \quad C_2 = \frac{\rho X_2^2}{2 g_c P_{D_0} t_0}\left[\left(\frac{A_p}{A_0}-1\right)^2+1\right]$$

$$C_3 = (1-\xi_0)^K + K(1-\xi_0)\xi_0^{K-1}$$

$$C_4 = K(1-\xi_0)^{K-1}$$

The maximum dimensionless pressure rise rate is given by:

$$\left.\frac{d\left(\frac{P_g}{P_{D_0}}\right)}{dt^*}\right|_{max} = 0.287\frac{C_4}{C_1\sqrt{C_2}} = 0.287(1-\xi_0)^{K-1}\frac{P_{D_0}}{P_{g_0}}\frac{t_0}{X_2}\left[\frac{2P_{D_0}}{\rho g_c\left[\left(\frac{A_p}{A_0}-1\right)^2+1\right]}\right]^{1/2} \tag{3}$$

For the linearized isentropic case with gas pressures in the range 15 to 2000 psia, K = 1.40, $\xi_0 = .95$. For the isothermal case, K = 1.

It is seen from Eq. 3 that the maximum dimensionless pressure rise rate is a function of the dimensionless number,

$$N = (1-\xi)^{K-1}\frac{P_{D_0}}{P_{g_0}}\frac{t_0}{X_2}\left[\frac{2P_{D_0}}{\rho g_c\left[\left(\frac{A_p}{A_0}-1\right)^2+1\right]}\right]^{1/2}$$

which depends upon:

(1) the driving pressure, P_d.

(2) the downstream pipe length, X_2.

(3) the pipe area to orifice area ratio, $\frac{A_p}{A_0}$.

(4) the nature of the compression process, whether it be isentropic or isothermal.

A comparison between the theoretical $\frac{d\,P_{3/P_0}}{dt}$ vs. time curve and the experimental pressure trace is shown in Fig. 5.

In Fig. 6 the maximum normalized pressure rise rate, , is plotted versus the number, $\frac{N}{t_o}$, with the reference time unit To equal to 1 sec.

3.2 Tests

A series of tests were run in order to verify the analysis. The following parameters were varied:

(1) Driving pressure - tests were run at 600, 1200, and 2000 psig.

(2) Orifice size - diameters of .070, .052, and .035 in. were used.

(3) The length of the downstream pipe section lengths of 60 and 33 in. were used.

For all tests the following parameters were held constant:

(1) Upstream pipe length = 184 in.

(2) Valve opening time = 16 m sec.

(3) Pipe inside diameter = .375 in.

3.3 Results and Discussion

Reasonable correlation between theoretical and experimental results was obtained as shown in Figs. 5 and 6. A comparison of the experimental and theoretical results shows that the compression of the air column is somewhere between isentropic and isothermal.

The parameter N in Eq. 3 is of interest since it reveals the variables influencing the maximum pressure rise rate. It is seen that the maximum pressure rise rate is directly proportional to the driving pressure raised to the 3/2 power, inversely proportion to the downstream pipe length, and varies in an inverse manner with the pipe to orifice area ratio. It is also influenced by the nature of the compression process, whether it be isentropic or isothermal.

It is important to note that the analysis developed assumes that the charging process is governed only by entrances and throttling losses. It remains to develop a method for determining under what conditions these assumptions may be used.

Future Work

1.) Combustion tests will be continued using Mil 2190 TEP in the 3/8 inch I.D. test section, both microfog and wick tests will be included.

2.) A series of napthenic neutral oils have been obtained with flash points varying between 300 and 500°F. These oils will be tested to determine the relative advantage, if any, of employing fluids with a higher flash point.

3.) Maximum temperature calculations will be made for the 3/8 inch I.D. test section in order to afford a comparison with the measured results similar to that given in this report.

4.) With regard to the liquid charging tests an effort will be made to ascertain under what condition the included analysis may be used.

5.) A study will be made to determine the maximum pressures attainable if combustion occurs during the liquid charging process.

References

1.) Progress Report No. 4. High Pressure Ignition, Contract No. Nobs 78674, March 31, 1961.

2.) Progress Report No. 8. High Pressure Ignition, Contract No. Nobs 78674, December 8, 1961.

3.) Progress Report No. 10. High Pressure Ignition, Contract No. Nobs 78674, April 5, 1962.

4.) H. E. Perlee and M. G. Zabetakis, Compressor and Related Explosions, Final Report No.3838, Bureau of Mines, Pittsburgh, Pennsylvania, September 15, 1961.

5.) Mathematical Tables from Handbook of Chemistry and Physics, Tenth Edition, Chemical Rubber Publishing Company.

Prepared by:

G. M. Faeth
Research Assistant
Mechanical Engineering

Approved by:

A. W. Hussmann
Professor of
Engineering Research

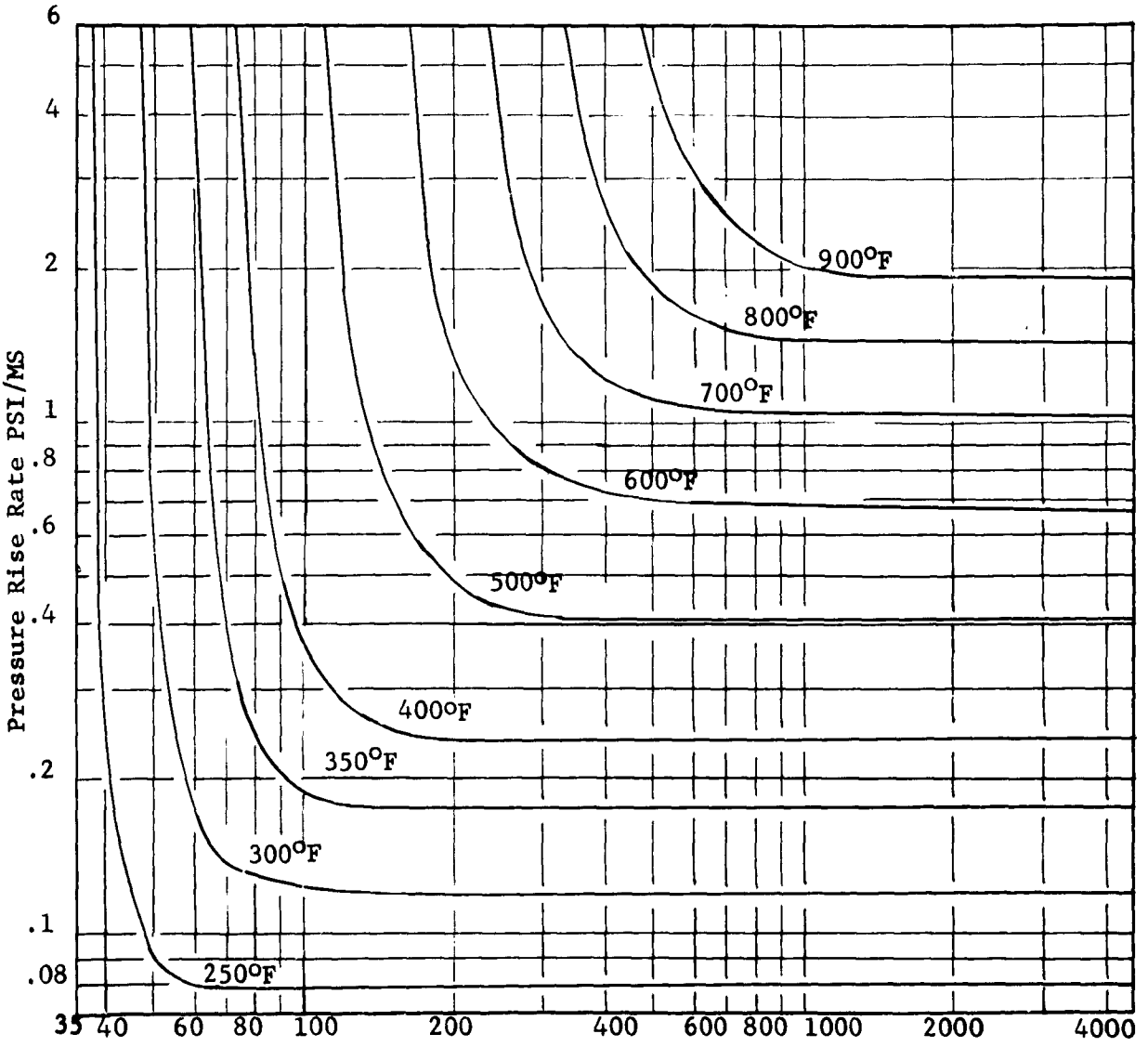

Fig. 1. Maximum Gas Temperatures in the Horizontal 7/8 inch I.D. Test Section.

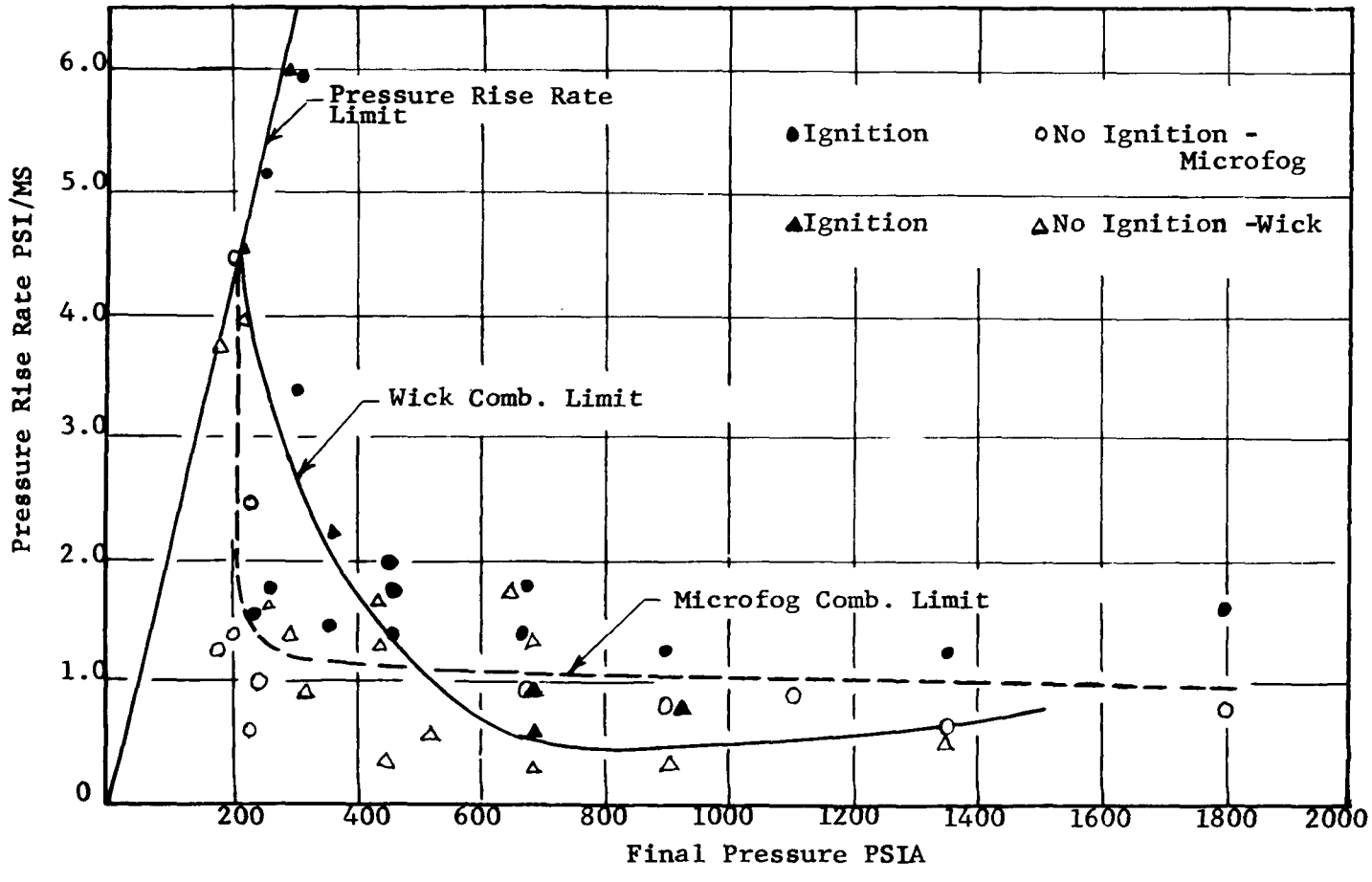

Fig. 2. Cetane Combustion Tests - 7/8 in. Horizontal Test Section 5' Long.

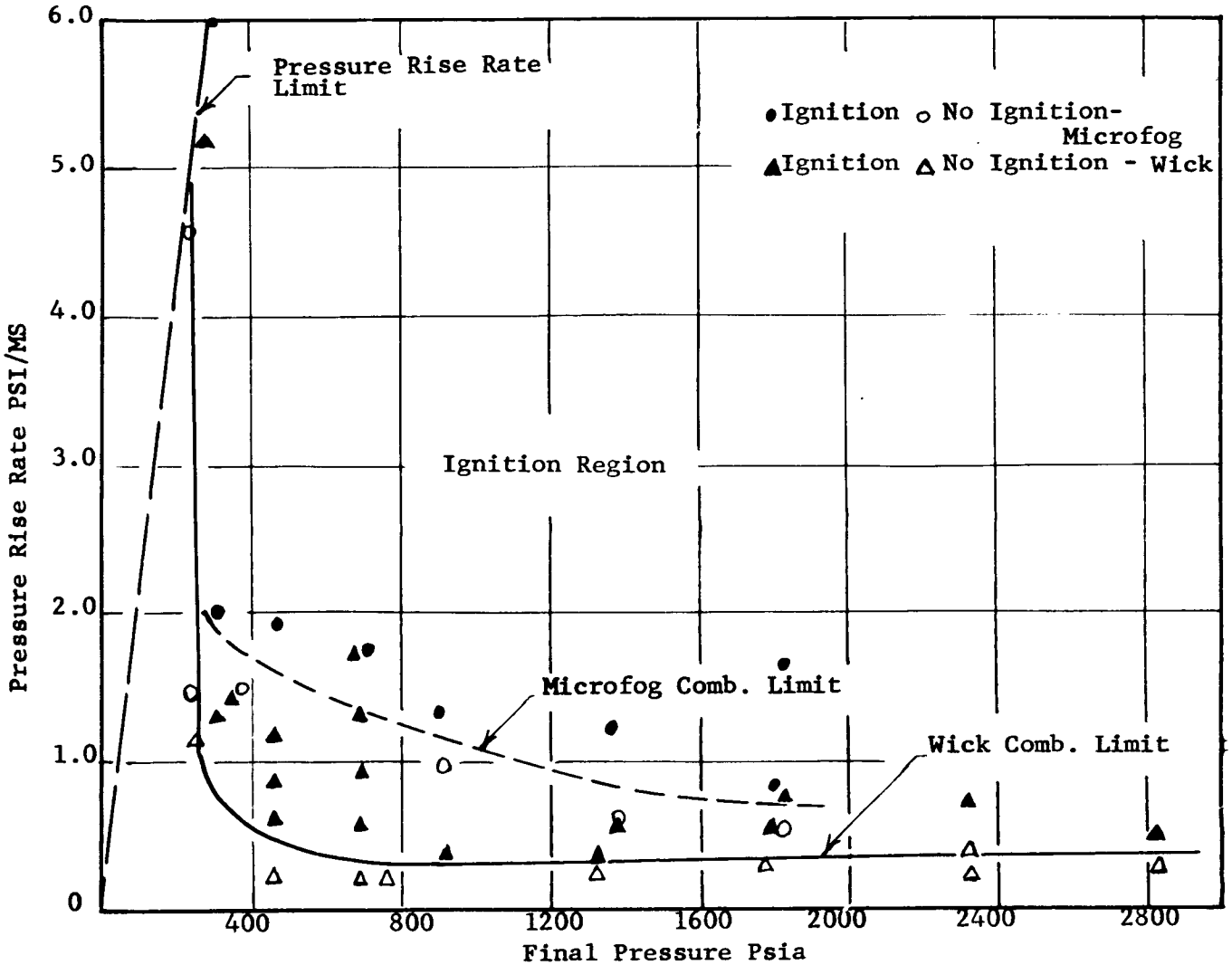

Fig. 3. MIL 2190 TEP Combustion Tests, 7/8 in. Horizontal Test Section 5' Long.

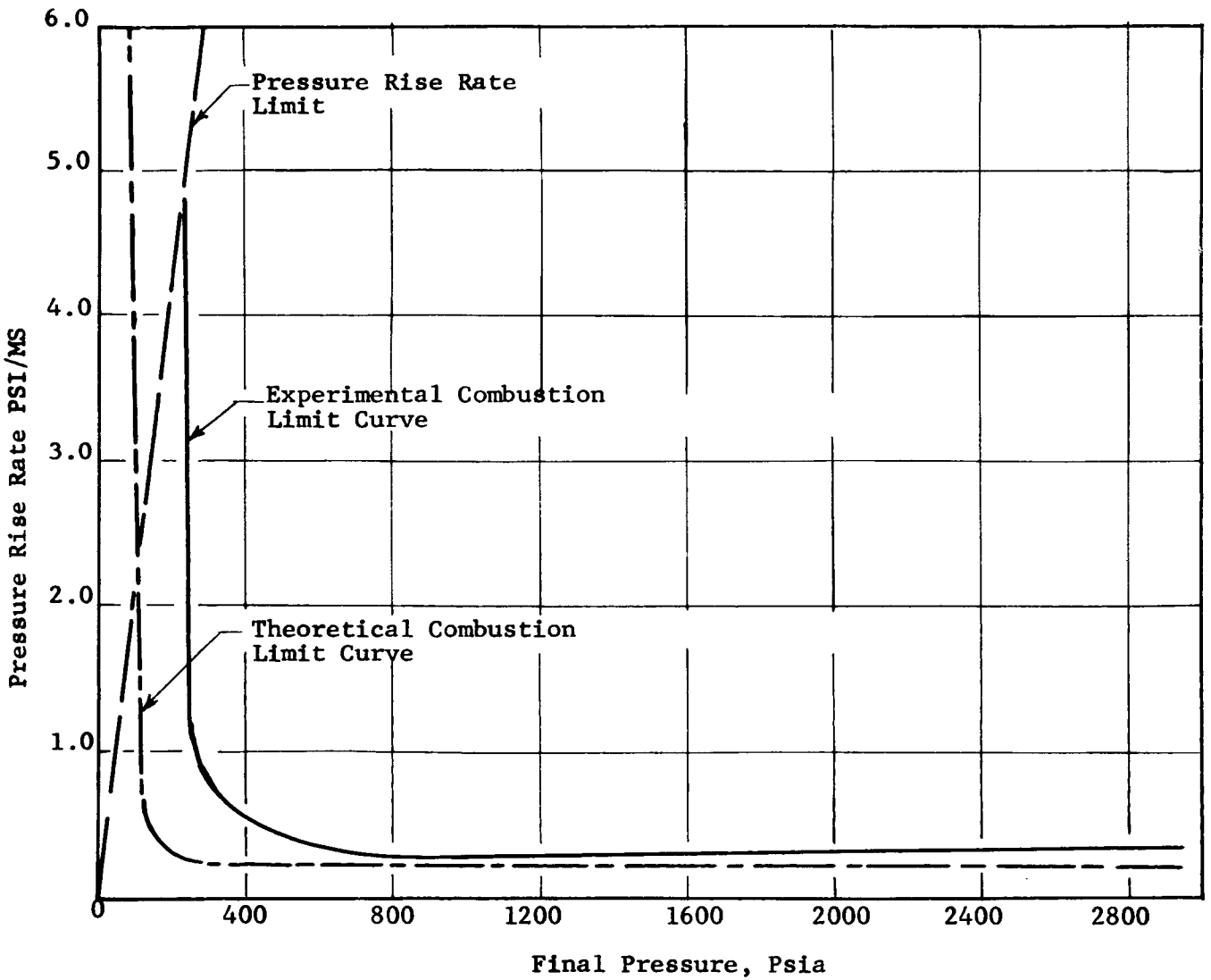

Fig. 4. Comparison of the Theoretical & Experimental Ignition Limits for MIL 2190 TEP - 7/8 inch Horizontal Test Section.

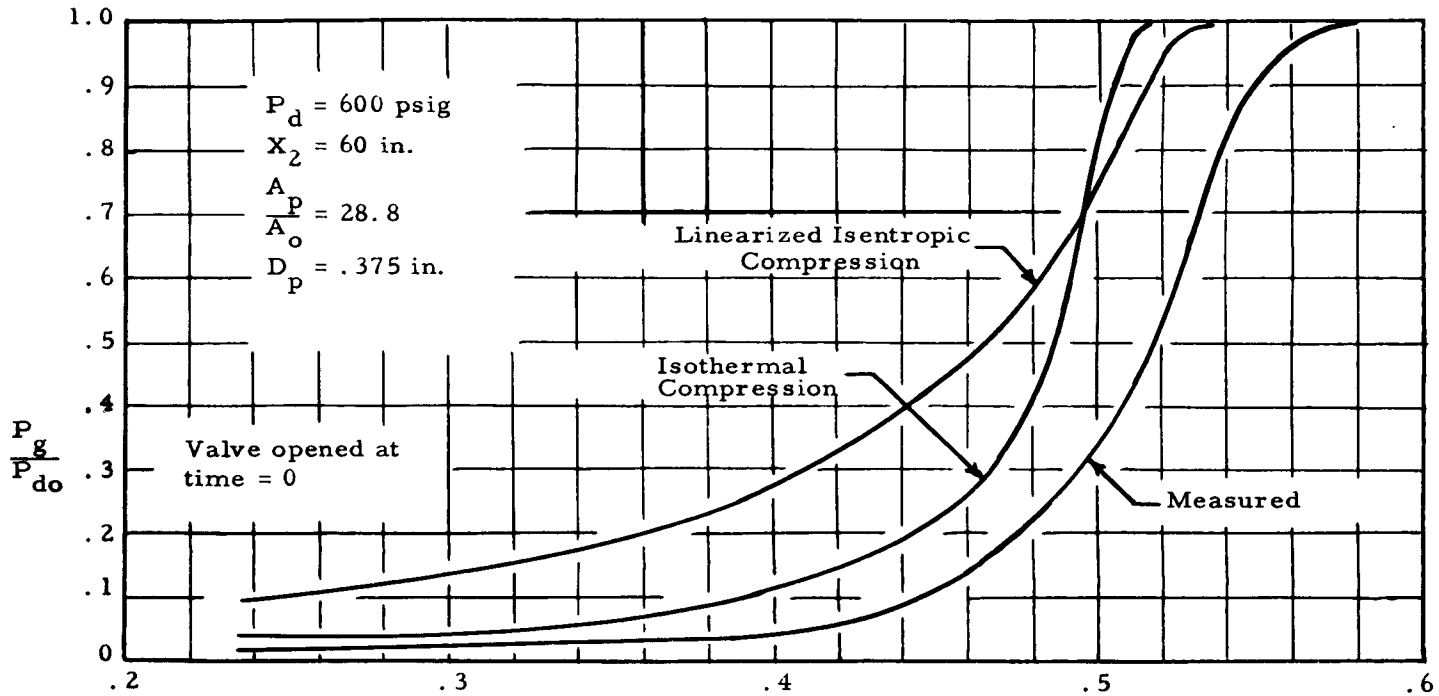

Fig. 5. Normalized Pressure vs Time

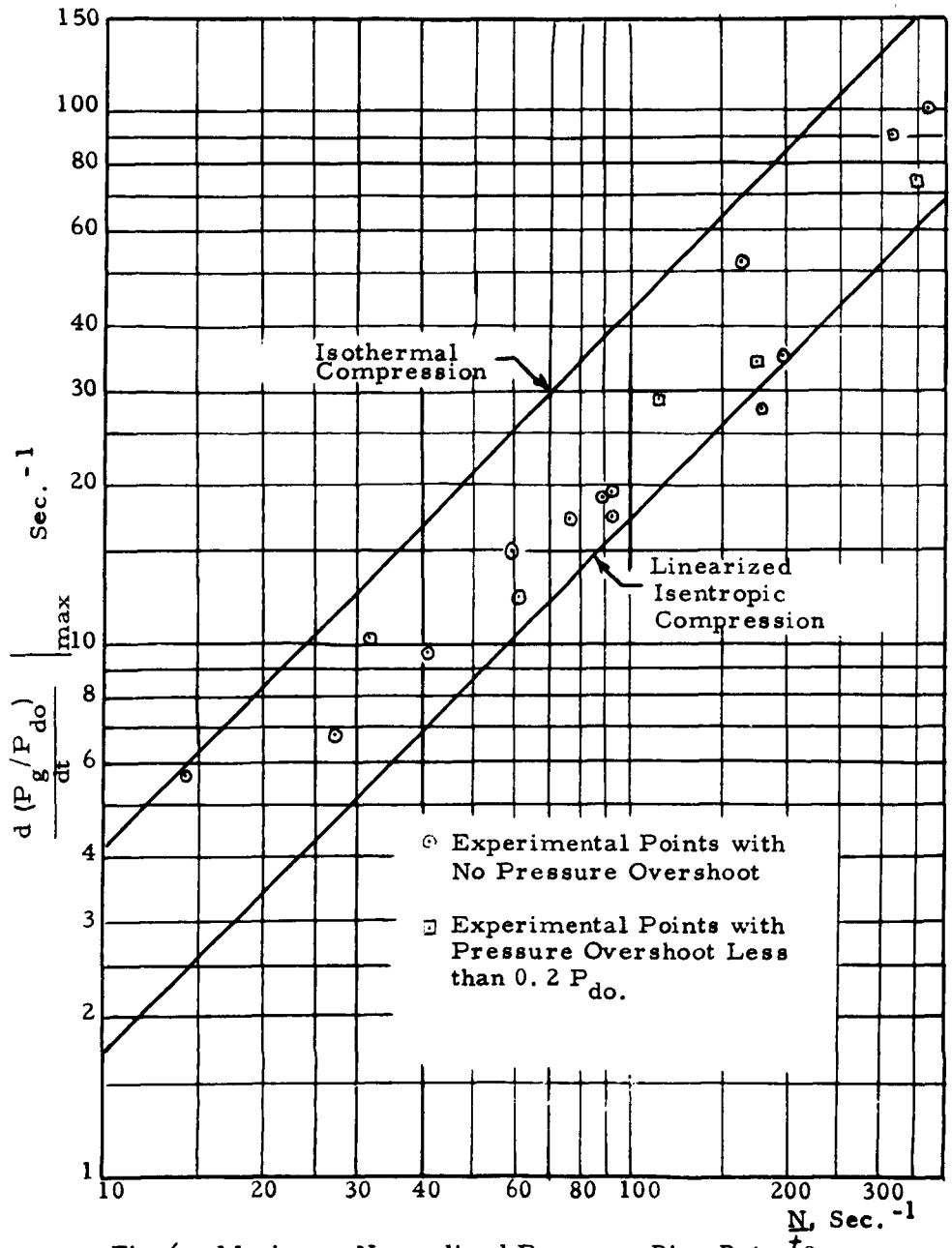

Fig. 6. Maximum Normalized Pressure Rise Rate $\frac{N}{t_o}$

vs.

$$\frac{N}{t_o} = .287\,(1-\xi_c)^{k-1}\,\frac{P_{do}}{P_{go}\,X_2}\left[\frac{2\,P_{do}}{\rho/g_c\,\left[(A_p/A_o-1)^2+1\right]}\right]^{.5}$$

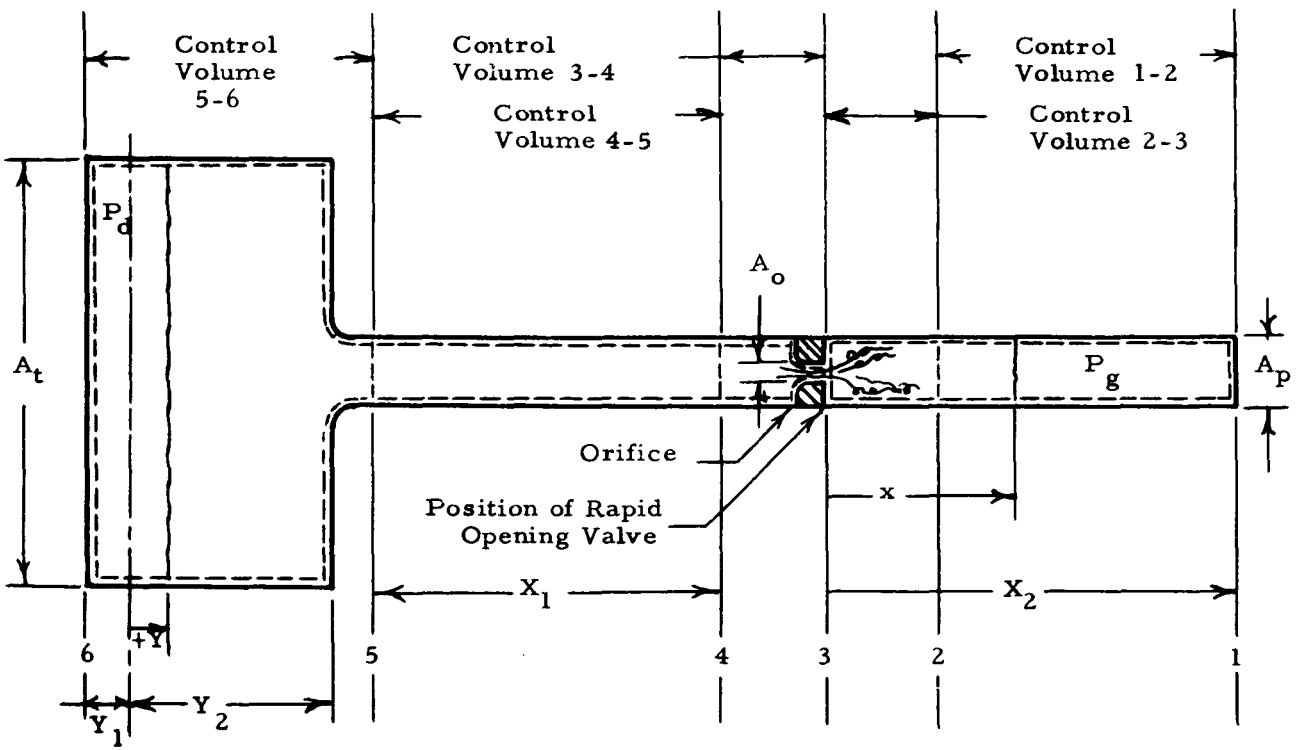

Fig. 7. Control Volumes Employed in Analysis

Appendix

Analysis of Liquid Charging Process

A-1 The analysis for the case where the process is governed only by entrance and throttling losses is presented with reference to Fig. 7.

A-2 Notation

A_o = cross sectional area of orifice, in^2.

A_p = cross sectional area of pipe, in^2.

A_t = cross sectional area of storage tank, in^2.

$d\bar{A}$ = differential area vector, in^3.

C_v = specific heat at constant volume for air. Btu/lb.

$C_1, C_2, C_3 \cdots$ = dimensionless constants defined throughout the analysis for ease of manipulation.

e = internal energy, in-lbf/lbm.

$\bar{F}_f$ = friction force, lb.

$\bar{F}$ = external force acting on a control volume, lb.

g_c = gravitational constant, $\frac{lbm}{lbf}\frac{in}{sec^2}$.

g = acceleration of gravity, in/sec^2.

h = enthalpy $\frac{in\text{-}lbf}{lbm}$

k = ratio of specific heats of air.

P_{go} = initial pressure of air in downstream pipe section, psia.

P_g = pressure of the air in the downstream pipe section, psia.

P_{do} = initial air pressure in the storage tank, psia.

P_d = air pressure in storage tank, psia.

$P_1, P_2, P_3, \cdots$ = pressure acting at control surfaces 1, 2, 3, ... respectively. See Fig. 7.

$\frac{d\left(\frac{P_3}{P_{0_0}}\right)}{dt}$ = normalized pressure rise rate, $sec.^{-1}$

$\frac{d\left(\frac{P_3}{P_{0_0}}\right)}{dt^*}$ = dimensionless pressure rise rate.

P_{shear} = the rate at which shear forces dissipate energy.

Q = the rate at which heat is transferred into a control volume.

t = time, sec.

t^* = dimensionless time parameter, = $\frac{t}{t_o}$

t_o = reference time unit, sec.

$\bar{v}$ = velocity of fluid particles, in/sec.

V = volume, in^3.

X_1, X_2, Y_1, Y_2 are defined in Fig. 7.

x = system coordinate = length of liquid column in downstream pipe section.

y = distance traveled by liquid level in tank, in.

z = elevation above an arbitrary datum, in.

ξ = dimensionless system coordinate, = $\frac{x}{X_2}$.

ξ_o = point about which the function $(1 - \xi)^k$ is linearized.

ρ = density of liquid, $\frac{lbm}{in^3}$.

ρ_g = density of gas, lbm/in^3.

A-3 Control Volume 1-2

The momentum equation is written in the form

$$\sum \vec{F} = \frac{\partial}{\partial t}\int_{C.V.} \frac{\rho}{g_c}\bar{v}\,dV + \oint_{C.S.} \frac{\rho}{g_c}\bar{v}\cdot d\bar{A}\,\bar{v} \qquad 1$$

which becomes

$$-F_{f1} + P_2 A_p - P_g A_p = \frac{\partial}{\partial t}\int_{x_1}^{x} \frac{\rho}{g_c}\frac{dx}{dt} A_p\,dx - \int_0^{A_p} \frac{\rho}{g_c}\left(\frac{dx}{dt}\right)^2 dA$$

where F_{f1} is the friction force exerted on the liquid by the pipe walls.
Carrying out the integration and differentiation gives,

$$P_2 = \frac{\rho}{g_c}\frac{d^2x}{dt^2}\left[x - x_1\right] + P_g + F_{f1} \qquad 2$$

Assuming that $F_{1f} = 0$ and that the effects of fluid acceleration are negligible, Eq. 2 becomes

$$P_2 = P_g \qquad 3$$

A-4 Control Volume 2-3

The momentum equation is again applied;

$$\sum \bar{F} = \frac{\partial}{\partial t}\int_{C.V.} \frac{\rho}{g_c}\,\bar{v}\,dV + \oint_{C.S.} \frac{\rho}{g_c}\,\bar{v}\cdot d\bar{A}\,\bar{v}$$

Assuming that the pressure acts uniformly over surface 3, the above reduces to,

$$-F_{f_2} + P_3 A_p - P_2 A_p = \frac{\partial}{\partial t}\int \frac{\rho}{g_c} v_x A_p\,dx + \int_0^{A_p} \frac{\rho}{g_c} v_2^2\,dA - \int_0^{A_o} \frac{\rho}{g_c} v_3^2\,dA$$

Neglecting friction and assuming quasi - steady conditions gives,

$$P_3 - P_2 = \frac{\rho}{g_c}\left[v_2^2 - v_3^2\,\frac{A_o}{A_p}\right] \qquad 4$$

For incompressible flow the continuity relation is

$$A_p v_2 = A_p \frac{dx}{dt} = A_o v_3$$

$$v_3 = \frac{A_p}{A_o}\frac{dx}{dt} \qquad 5$$

Substituting Eq. 5 into Eq. 4 gives,

$$P_3 - P_2 = \frac{\rho}{g_c}\left(\frac{dx}{dt}\right)^2\left[1 - \frac{A_p}{A_o}\right] \qquad 6$$

A-5 Control Volume 3-4

The energy equation is written in the form,

$$Q + P_{shear} + \frac{\partial}{\partial t}\int_{C.V.}\frac{\rho}{g_c} e\, dV + \int_{C.S.}\left[h + \frac{v^2}{2g_c} + \frac{zg}{g_c}\right]\rho\, \bar{v}\cdot d\bar{A} \qquad 7$$

Assuming, $Q = P_{shear} = z = o$, the internal energy of the liquid remains constant and quasi-steady state conditions, Eq. 6 reduces to,

$$0 = \oint_{C.S.}\left(\frac{P}{\rho} + \frac{v^2}{2g_c}\right)\rho\, \bar{v}\cdot d\bar{A}$$

which becomes

$$0 = -\left[\frac{P_4}{\rho} + \frac{V_4^2}{2g_c}\right]\rho V_4 A_p + \left[\frac{P_3}{\rho} + \frac{V_3^2}{2g_c}\right]\rho V_3 A_o \qquad 8$$

The continuity relation is

$$A_o V_3 = A_p V_4 = A_p \frac{dx}{dt}$$

Therefore Eq. 8 reduces to

$$P_3 - P_4 = \frac{\rho}{2 g_c}\left(\frac{dx}{dt}\right)^2\left[1 - \left(\frac{A_o}{A_p}\right)^2\right] \qquad 9$$

A-6 Control Volume 4-5

The momentum equation is

$$\sum F = \frac{\partial}{\partial t}\int_{C.V.} \frac{\rho}{g_c}\,\bar{v}\,dV + \oint_{C.S.} \frac{\rho}{g_c}\,\bar{v}\cdot d\bar{A}\,\bar{v}$$

which reduces to

$$P_5 A_p - P_4 A_p - F_{f3} = \frac{\partial}{\partial t}\int_{-X_1}^{0} \frac{\rho}{g_c}\frac{dx}{dt} A_p dx - \int_{0}^{A_p} \frac{\rho}{g_c}\left(\frac{dx}{dt}\right)^2 + \int_{0}^{A_p} \frac{\rho}{g_c}\left(\frac{dx}{dt}\right)^2 dH \qquad 10$$

Neglecting friction and assuming the effects of fluid acceleration negligible Eq. 10 becomes

$$P_5 = P_4 \qquad 11$$

A-7 Control Volume 5-6

The energy equation is written in the form

$$Q = P_{Shear} + \frac{\partial}{\partial t}\int_{C.V.} e\,\rho\,dV + \int_{C.S.}\left(h + \frac{V^2}{2g_c} + z\frac{g}{g_c}\right)\rho\,\bar{v}\cdot d\bar{A} \qquad 12$$

The following assumptions are made:

(1) Kinetic energy of the gas is negligible.

(2) Internal energy of the liquid remains constant.

(3) Elevation effects are negligible

(4) $Q = P_{shear} = 0$

Eq. 12 then reduces to

$$0 = \frac{\partial}{\partial t}\int_{-Y_1}^{y} \rho_g u_g A_t\,dy + \frac{\partial}{\partial t}\int_{y}^{Y_2}\frac{\left(\frac{dy}{dt}\right)^2}{2g_c}\rho A_t\,dy + \int_{0}^{A_p}\left(\frac{p_s}{\rho} + \frac{\left(\frac{dx}{dt}\right)^2}{2g_c}\right)\rho\frac{dx}{dt}\,dA$$

Carrying out the integration gives,

$$0 = \frac{\partial}{\partial t}\left[\rho_g u_g A_t (y + Y_1)\right] + \frac{\partial}{\partial t}\left[\frac{\left(\frac{dy}{dt}\right)^2}{2g_c}\rho\,(Y_2 - y)\right] + \left[\frac{p_s}{\rho} + \frac{\left(\frac{dx}{dt}\right)^2}{2g_c}\right]\rho\frac{dx}{dt}A_p \qquad 13$$

Assuming an ideal gas it follows that

$$u_g = c_v T$$

$$\rho_g U_g = \frac{C_v P}{R} = \frac{P}{K-1} \qquad 14$$

The gas in the air tank is assumed to expand isentropically hence,

$$P_D = P_{D_o}\left[\frac{V_1}{y+V_1}\right]^K \qquad 15$$

Substituting Eqs. 15 & 14 into Eq. 13 and differentiating gives;

$$\frac{1-K}{K-1} P_{D_o} V_1^K A_t [y+V_1]^{-K} \frac{dy}{dt} + \frac{\rho}{g_c} A_t \frac{dy}{dt}\left[\frac{d^2y}{dt^2}(V_2-y) - \frac{\left(\frac{dy}{dt}\right)^2}{2}\right] +$$

$$+\left[\frac{P_5}{\rho} + \frac{\left(\frac{dx}{dt}\right)^2}{2g_c}\right]\rho \frac{dx}{dt} = 0 \qquad 16$$

Neglecting the effects of fluid acceleration and employing the continuity relation $A_t \frac{dy}{dt} = A_p \frac{dx}{dt}$, Eq. 16 becomes

$$0 = -\frac{P_{D_o} V_1^K}{(y+V_1)^K} + \frac{\rho}{2g_c}\left(\frac{dx}{dt}\right)^2 + P_5 \qquad 17$$

Assuming that y is always small compared to Y_1, ie $Y_1 + y \approx \bar{Y}_1$ Eq. 17 reduces to,

$$P_{D_o} - P_s = \frac{\rho}{2g_c}\left(\frac{dx}{dt}\right)^2 \qquad 18$$

A-8 System Differential Equation
Combining Eqs. 18, 11, 9, 6, and 3 gives

$$1 - \frac{P_g}{P_{D_o}} = \frac{\rho\left(\frac{dx}{dt}\right)^2}{2g_c P_{D_o}}\left[\left(\frac{A_p}{A_o} - 1\right)^2 + 1\right] \qquad 19$$

The air column in the downstream pipe section is assumed to be compressed isentropically, hence

$$P_g = P_{g_o}\left[\frac{\bar{X}_2}{\bar{X}_2 - x}\right]^K \qquad 20$$

Eq. 20 is substituted into Eq. 19 and the resulting equation is put into dimensionless form giving

$$1 - \frac{P_{g_0}}{P_{D_0}} \frac{1}{(1-\xi)^K} = \frac{\rho X_2^2}{2 g_c P_{D_0} t_0^2} \left[\left(\frac{A_p}{A_0} - 1 \right)^2 + 1 \right] \left(\frac{d\xi}{dt^*} \right)^2 \qquad 21$$

where

$$\xi = x X_2 \qquad t^* = t_0 t \quad , \quad t_0 = \text{reference time unit}$$

For ease of manipulation, C_1 and C_2 are defined as

$$C_1 = \frac{P_g}{P_{D_0}} \qquad C_2 = \frac{\rho X_2^2}{2 g_c P_{D_0} t_0^2} \left[\left(\frac{A_p}{A_0} - 1 \right)^2 + 1 \right]$$

and Eq. 21 takes the form

$$1 - \frac{C_1}{(1-\xi)^K} = C_2 \left(\frac{d\xi}{dt^*} \right)^2 \qquad 22$$

The initial condition for the system is

$$\xi = 0 \quad \text{at} \quad t^* = 0$$

A-9 Solution of the Differential Eq. 22

The function, $(1-\xi)^k$ is linearized by the use of a Taylor Series expansion, neglecting higher order terms

$$f(\xi) = (1-\xi)^K$$

$$f(\xi) \sim f(\xi_0) + f'(\xi_0)(\xi - \xi_0) + \cdots$$

$$f(\xi) \sim (1-\xi_0)^K - K(1-\xi_0)^{K-1}(\xi - \xi_0)$$

$$f(\xi) \sim (1-\xi_0)^K + K(1-\xi_0)^{K-1}\xi_0 - K(1-\xi_0)^{K-1}\xi \qquad 24$$

Eq. 24 is then of the form

$$f(\xi) = (1-\xi)^K \sim C_3 - C_4\xi \qquad 25$$

where

$$C_3 = (1-\xi_0)^K + K(1-\xi_0)^{K-1}\xi_0$$

$$C_4 = K(1-\xi_0)^{K-1}$$

Eq. 22 may be written as

$$\frac{\sqrt{C_2}\, d\xi}{\sqrt{1 - \frac{C_1}{C_3 - C_4\xi}}} = dt^* \qquad 26$$

Eq. 26 is integrated by performing the following transformation:

Let

$$\frac{c_1}{c_3 - c_4 \xi} = \sin^2\theta \qquad 27$$

$$\left(\frac{c_1 c_4}{(c_3 - c_4\xi)^2}\right) d\xi = 2\sin\theta\cos\theta\, d\theta$$

$$d\xi = 2\sin\theta\cos\theta \frac{(c_3 - c_4\xi)^2}{c_4 c_1} d\theta$$

$$d\xi = 2\frac{c_1}{c_4}\frac{\cos\theta}{\sin^3\theta} d\theta$$

Eq. 26 now becomes

$$\frac{2\sqrt{c_2}\,\frac{c_1}{c_4}\,\frac{\cos\theta}{\sin^3\theta}\, d\theta}{\sqrt{1 - \sin^2\theta}} = dt^*$$

or

$$\frac{2\sqrt{c_2}\, c_1}{c_4}\,\frac{d\theta}{\sin^3\theta} = dt^* \qquad 28$$

The Boundary conditions of Eq. 23 are:

$$\xi = 0 \text{ at } t^* = 0$$

From Eq. 27 it follows

$$C/C_3 = \sin^2\theta \quad at \quad t^* = 0$$

or

$$\theta = \sin^{-1}\sqrt{\frac{C_1}{C_3}} \quad at \quad t^* = 0 \qquad 29$$

Eq. 28 is now integrated with the following formula (Ref. 5):

$$\int \frac{d\theta}{\sin^3\theta} = \left[-\frac{1}{2}\frac{\cos\theta}{\sin^2\theta} + \frac{1}{2}\ln\left(\tan\frac{\theta}{2}\right)\right] + \text{constant}$$

Integrating Eq.28 with conditions 29 gives

$$\frac{2\sqrt{C_2 C_1}}{C_4}\int_{\sin^{-1}\sqrt{\frac{C_1}{C_3}}}^{\theta} \frac{d\theta}{\sin^3\theta} = \frac{\sqrt{C_2 C_1}}{C_4}\left[-\frac{\cos\theta}{\sin^2\theta} + \ln\left(\tan\frac{\theta}{2}\right)\right]_{\sin^{-1}\sqrt{\frac{C_1}{C_3}}}^{\theta} = t^*\Big|_0^{t^*} \qquad 30$$

Putting in the limits and employing the appropriate trigonometric formulas gives,

$$\frac{C_1\sqrt{C_2}}{C_4}\left[-\frac{\cos\theta}{\sin^2\theta} + \ln\left(\tan\frac{\theta}{2}\right)\right] + \sqrt{C_2}\left[\frac{C_3}{C_4}\sqrt{1-\frac{C_1}{C_3}} + \frac{C_1}{C_3}\ln\frac{\sqrt{\frac{C_1}{C_3}}}{1+\sqrt{1-\frac{C_1}{C_3}}}\right] = t^* \qquad 31$$

From Eqs. 27, 25, 22, 21, and 19, it follows that

$$\sin^2\theta = \frac{C_1}{C_3 - C_4\xi} \sim \frac{C_1}{(1-\xi)^k} = \frac{P_g}{P_{D_o}}, \quad \sin^{-1}\sqrt{\frac{C_1}{C_3}} \leq \theta \leq \frac{\pi}{2} \qquad 32$$

Eqs. 31 and 32 form a solution from which the $\frac{P_g}{P_{D_o}}$ vs t curve may be constructed. The solution assumes a linearized representation of the function, $(1 - \xi)^k$, about the point ξ_o. Depending upon the range of pressure involved, the point ξ_o will vary. A value of $\xi_o = 0.95$ was used in the calculations and the function $(1-\xi)^k$ was represented quite well in the range $0 \leq \xi \leq .95$ which corresponds to a pressure range for the air column of 15 to 2000 psia.

A-10 Isothermal Compression of the Air Column

The solution for this case is found by noting that for an isothermal compression the air pressure is given by:

$$P_g = P_{g_o}\frac{X_2}{X_2 - X} \qquad 33$$

and in dimensionless form

$$P_g = \frac{P_{g_o}}{(1-\xi)} \qquad 34$$

Comparing Eq. 33 with Eq. 20 it follows that the solution given by Eq. 31 and 32 reduces to the isothermal case if $k = 1$.

A-11 Maximum Pressure Rise Rate

Recalling Eq. 32 it is seen that

$$\frac{P_q}{P_{D_0}} = \sin^2\theta \qquad \text{(repeated) 32}$$

Differentiating with respect to t^* gives

$$\frac{d\left(\frac{P_q}{P_{D_0}}\right)}{dt^*} = 2\sin\theta\cos\theta\,\frac{d\theta}{dt^*} \qquad 35$$

$\frac{d\theta}{dt^*}$ is obtained by differentiating Eq. 31 implicitly and upon substitution into Eq. 35 gives,

$$\frac{d\left(\frac{P_q}{P_{D_0}}\right)}{dt^*} = \frac{2\sin\theta\cos\theta}{\left[\frac{1}{\sin\theta} + \frac{2\cos^2\theta}{\sin^3\theta} + \frac{\sec^2\frac{\theta}{2}}{2\tan\frac{\theta}{2}}\right]}\,\frac{C_4}{C_1\sqrt{C_2}} \qquad 36$$

Noting that $\frac{\sec^2\frac{\theta}{2}}{2\tan\frac{\theta}{2}} = \frac{1}{\sin\theta}$ Eq. 36 reduces to

$$\frac{d\left(\frac{P_q}{P_{D_0}}\right)}{dt^*} = \sin^4\theta\cos\theta\,\frac{C_4}{C_1\sqrt{C_2}} \qquad 37$$

The maximum value of $\frac{d\frac{P_g}{P_a}}{dt^*}$ is determined by maximizing the function, $\sin^4\theta\cos\theta\frac{C_4}{C_1\sqrt{C_2}}$ with respect to the parameter θ. A necessary condition for the maximum is

$$\frac{d}{d\theta}(\sin^4\theta\cos\theta) = 0 \qquad 38$$

Differentiating using the product rule gives

$$4\sin^3\theta\cos^2\theta - \sin^5\theta = 0$$

$$\cos\theta = \sqrt{.2}$$

$$\theta = 63.3^\circ \qquad 39$$

The fact that the above value of θ determines a maximum is verified by the fact that the second derivative

$$\frac{d^2}{d\theta^2}(\sin^4\theta\cos\theta) = -10\cos\theta\sin\theta$$

is always negative for the admissible range of θ Substituting the value of θ determined by Eq. 39 into Eq. 37 gives

$$\left.\frac{d\left(\frac{P_g}{P_a}\right)}{dt^*}\right|_{max} = 0.287\frac{C_4}{C_1\sqrt{C_2}} \qquad 40$$

A-12 Summary

1. The $\frac{P_g}{P_{D_o}}$ vs. t curve is constructed from the following:

$$\frac{c_1\sqrt{c_2}}{c_4}\left[-\frac{\cos\theta}{\sin^2\theta}+\ln\left(\tan\frac{\theta}{2}\right)\right]+$$

$$+\sqrt{c_2}\left[\frac{c_3}{c_4}\sqrt{1-\frac{c_1}{c_3}}+\frac{c_1}{c_3}\ln\frac{\sqrt{\frac{c_1}{c_3}}}{1+\sqrt{1-\frac{c_1}{c_3}}}\right]=t^* \qquad 41$$

$$\sin^2\theta=\frac{P_g}{P_{D_o}}\ ,\quad \sin^{-1}\sqrt{\frac{c_1}{c_3}}\leq\theta\leq\frac{\pi}{2} \qquad 42$$

where

$$c_1=\frac{P_{g_o}}{P_{D_o}}\ ,\quad c_2=\frac{\rho\dot{X}_z^2}{2g_c P_{D_o} t_o^2}\left[\left(\frac{A_p}{A_o}-1\right)^2+1\right]$$

$$c_3=(1-\xi_c)^K+K(1-\xi_o)^{K-1}\xi_o$$

$$c_4=K(1-\xi_o)^{K-1}$$

2. The maximum pressure rise rate is given by

$$\frac{d\left(\frac{P_g}{P_{D_o}}\right)}{dt^*}=.287\frac{c_4}{c_1\sqrt{c_2}}=0.287(1-\xi_o)^{K-1}\frac{P_{D_o}}{P_{g_o}}\frac{t_o}{\dot{X}_z}\left[\frac{2P_{D_o}}{\rho g_c\left[\left(\frac{A_p}{A_o}-1\right)^2+1\right]}\right]^{\frac{1}{2}} \qquad 43$$

3. For the linearized isentropic case with gas pressures in the range 15 to 2000 psia, $k = 1.40$ and $\xi_o = .95$ were used in the calculations.

4. For the isothermal case, $k = 1.0$.